Insulator-metal transition and giant magnetoresistance in $La_{1-x}Sr_xMnO_3$

A. Urushibara
Department of Physics, University of Tokyo, Tokyo 113, Japan

Y. Moritomo*
Joint Research Center for Atom Technology (JRCAT), Tsukuba 305, Japan

T. Arima
Department of Physics, University of Tokyo, Tokyo 113, Japan

A. Asamitsu
Joint Research Center for Atom Technology (JRCAT), Tsukuba 305, Japan

G. Kido
National Research Institute for Metals, Tsukuba 305, Japan

Y. Tokura
Department of Physics, University of Tokyo, Tokyo 113, Japan
and Joint Research Center for Atom Technology (JRCAT), Tsukuba 305, Japan
(Received 20 January 1995)

Insulator-metal phenomena depending on band filling (doping degree), temperature, and external magnetic field have been investigated for prototypical double-exchange ferromagnets, namely, crystals of $La_{1-x}Sr_xMnO_3$ ($0 \leq x \leq 0.6$). The electronic phase diagram in the plane of the temperature vs nominal hole concentration (x) has been deduced from the magnetic and electrical measurements on the melt-grown crystals. Around the ferromagnetic transition temperature T_C, large negative magnetoresistance was observed. Irrespective of temperature, reduction of the resistivity is scaled with the field-induced magnetization (M) as $-\Delta\rho/\rho = C(M/M_s)^2$ for $M/M_s \lesssim 0.3$, where M_s is the saturated magnetization. The coefficient C strongly depends on x, i.e., $C \approx 4$ near the compositional insulator-metal phase boundary ($x_c \sim 0.17$), but decreases down to ≈ 1 for $x \geq 0.4$, indicating the critical change of the electronic state.

I. INTRODUCTION

The discovery of high-temperature superconductivity in hole-doped copper oxide compounds has aroused renewed and extended interest in the correlated dynamics of spins and charges near the metal-insulator transition in $3d$ transition-metal oxides with strong electron correlation. In the course of the studies, electronic properties of hole-doped manganese oxides with perovskite structure, $R_{1-x}A_xMnO_3$ (R being rare-earth ions and A divalent ions, e.g., A=Ca, Sr, Ba, and Pb),[1] have been revisited and large magnetoresistance (MR) phenomena have been reported.[2–8] In this paper, we report a comprehensive study on the correlation between the electrical and magnetic properties in crystals of $La_{1-x}Sr_xMnO_3$ with various hole concentrations (x). A part of the results of the MR effects for the x=0.175 crystal have been published.[8] Here, we describe the whole feature of the x-dependent electronic and magnetotransport properties in crystals of $La_{1-x}Sr_xMnO_3$ ($0.0 \leq x \leq 0.6$).

The ferromagnetic state in these manganese oxides has long been known as a prototypical example for the double-exchange interaction.[9–12] The Mn^{3+} ion in nominally hole-undoped $LaMnO_3$ has the electron configuration of $t_{2g}^3 e_g^1$. The end insulator $LaMnO_3$ is a charge-transfer (CT) insulator, in which the gap transition corresponds to the CT excitation from O $2p$ to Mn $3d$ state.[13] Among the four $3d$ electrons on the Mn site, t_{2g}^3 electrons may be viewed as a local spin (S=3/2) because of relatively poor hybridization with O $2p$ states, while the strongly hybridized e_g^1 state is either itinerant or localized as the case may be. Deviation of the e_g band filling ($n = 1-x$) from n=1, or the so-called hole doping, causes an insulator-metal transition.[14] A distinct feature of such a barely metallic state in the manganese oxides is that there is strong exchange interaction (J; Hund coupling) between the itinerant e_g electrons (or holes) and the local t_{2g} spins. The interplay between the configuration of the local spins and the dynamics of the e_g carriers governs the electronic properties including the temperature and magnetic field-dependent metal-nonmetal phenomena. After the pioneering works on ceramics of $La_{1-x}Ca_xMnO_3$ and $La_{1-x}Sr_xMnO_3$,[14–16] Searle and Wang[17] reported in 1969 the first MR measurements on a flux-grown single crystal of $La_{1-x}Pb_xMnO_3$ (x=0.31). Kubo and Ohata[9]

0163-1829/95/51(20)/14103(7)/$06.00

derived the expression of the temperature and magnetic field dependence of the resistivity using the Drude approximation on the basis of the Kondo lattice model with ferromagnetic coupling ($J \geq 0$). Recently, Furukawa[18] has calculated the resistivity as a function of the magnetization using the Kubo formula in the limit of the classical spin ($S=\infty$) and infinite dimension ($D=\infty$) for the Kondo lattice model, and given a mean-field interpretation to the problem why the MR in the hole-doped manganates can be so large.

Here, we present the experimental investigation on the MR effect with particular emphasis on its conspicuous filling (or nominal hole concentration) dependence, which is to be elucidated perhaps beyond the mean-field approximation. To correlate the charge dynamics with the spin dynamics, a high-quality crystal is needed. This is partly because the ceramics sample suffers from the carrier scattering at the grain boundaries, where the modifications of the microscopic magnetic structures likely take place. In fact, the metal-nonmetal phenomena as well as the magnetotransport properties of the crystal differ considerably from those of the ceramics samples. Another important fact to be noticed is that the electronic and magnetic properties critically depend on x in the hole-doped Mn oxide, and hence the finely and systematically filling-controlled samples are indispensable for the detailed investigation. For this purpose, we have grown crystals of $La_{1-x}Sr_xMnO_3$ with controlled band filling ($0 \leq x \leq 0.6$) by the floating-zone (FZ) method.

The format of the present paper is as follows. In Sec. II, we describe details of the crystal growth with use of a FZ furnace as well as measurements for the resistivity and magnetization under magnetic field up to 15 T. The overall electronic phase diagram for $La_{1-x}Sr_xMnO_3$ as a function of x is presented in Sec. III on the basis of the results of the simultaneous electrical and magnetic measurements. The static magnetic structure in $La_{1-x}Ca_xMnO_3$ and related compounds have been thoroughly investigated for the ceramics samples so far,[14–16] yet the correlation between the spin dynamics/structures and charge transport properties was left to be clarified. Section IV is devoted to the magnetotransport properties. We describe the results of the MR measurements with a magnetic field up to 15 T. The magnitude of the negative MR, defined by $-[\rho(H)-\rho(0)]/\rho(0)$, reaches as large a value as 0.95 around T_C for the ferromagnetic phase transition. Furthermore, x-dependent behavior of the MR is argued in terms of the mean-field-type interpretation of the Kondo-lattice model with ferromagnetic coupling ($J \geq 0$), and interpreted as a crossover of the system from strong coupling ($J \gg W$, where W is the one-electron bandwidth) to weak coupling regime with increase of x. The summary is given in Sec. V.

II. EXPERIMENTAL

Crystals of $La_{1-x}Sr_xMnO_3$ were grown by the FZ method. The starting materials were La_2O_3, $SrCO_3$, and $MnCO_3$. La_2O_3 was fired in air at 1200 °C for 12 h before use. $MnCO_3$ was also calcined in air at 1200 °C for 12 h to form Mn_3O_4, which is the most stable compound in the Mn-O systems. Then, the raw materials were weighted to a prescribed ratio, mixed, and stirred with acetone for 1 h in a ball mill. The mixture was heated at 1200 °C for 24 h in air. The prereacted materials were then pulverized and mixed again. After this process, a feed rod was formed to a cylindrical shape of about 5 mm in diameter and 80 mm in length with pressure of 2 ton/cm^2 and heated at 1200 °C in air for 12 h. The apparatus used for the crystal growth was the FZ furnace equipped with two halogen incandescent lamps and hemielliptic focusing mirrors. The feed and seed rods were rotated in opposite directions at a relative rate of 50 rpm and the melted zone was vertically scanned at a speed of 8–10 mm/h. The atmosphere during the crystal growth was changed with the crystal composition; in a flow of argon gas for x=0, 0.05, air for x = 0.1–0.25, and a mixture of oxygen and argon gas for x = 0.3–0.6. Those conditions adopted for the crystal growth are summarized in Table I together with the Néel temperature (T_N), the Curie temperature (T_C), and the saturated magnetization (M_s). T_C was determined from temperature dependence of ac susceptibility. The crystal structure was examined by x-ray powder diffraction with Cu $K\alpha$ radiation, which indicated that all the samples were single phase. The crystal structure at room temperature changes from orthorhombic ($Pbnm$, Z=4; $x < 0.175$) to rhombohedral ($R\bar{3}c$, Z=2; $x \geq 0.175$). The change of the lattice parameters is shown against x in Fig. 1. Analyses of chemical composition were carried out using an electron probe microanalyzer (EPMA), redox titration, and thermogravimetry (see Table I). The obtained crystals with $0 \leq x \leq 0.4$ show the nearly identical composition with the prescribed one.

Resistivity measurements were performed using the conventional four-probe method. Electrodes were formed with heat treatment type silver paint. The sample was cut into a rectangular shape, with the typical dimension of 3×1×0.5 mm^3. The high-temperature measurements above 300 K were conducted in an atmosphere of N_2. Magnetization (M) was measured with a superconducting quantum interference device magnetometer ($\mu_0 H \leq 5$ T). Measurements of M at higher fields ($\mu_0 H \leq 15$ T)

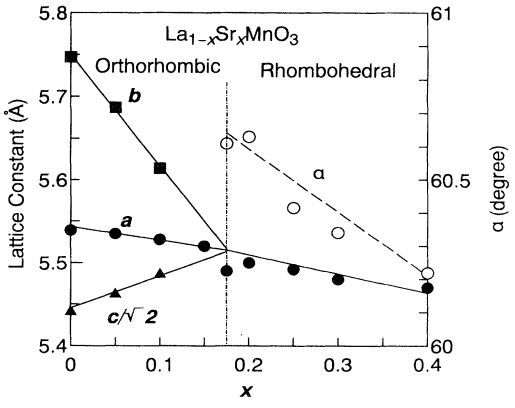

FIG. 1. Lattice parameters for $La_{1-x}Sr_xMnO_3$ crystals at room temperature.

TABLE I. Conditions for the crystal growth by the FZ method and results of the characterization of $La_{1-x}Sr_xMnO_3$. $\%Mn^{4+}$ shows the nominal Mn valence of the obtained crystal (ideally x for the stoichiometric sample) obtained by the redox titration. EPMA indicated that the metal composition (La/Sr/Mn) is nearly identical with the prescribed one within the experimental accuracy of ±2%. T_N, T_C, and M_s mean the Néel temperature, the Curie temperature, and the saturated magnetization, respectively.

x	Method	Atmosphere	$\%Mn^{4+}$	T_N (K)	T_C (K)	Structure	M_s (μ_B/Mn site)
0.00	FZ	Ar	2	143		Orthorhombic	
0.05	FZ	Ar	7	139		Orthorhombic	
0.10	FZ	air	12		145	Orthorhombic	3.6
0.15	FZ	air	15		238	Orthorhombic	4.2
0.175	FZ	air	17		283	Rhombohedral	4.0
0.20	FZ	air	19		309	Rhombohedral	3.9
0.25	FZ	air	19		342	Rhombohedral	3.9
0.30	FZ	Ar 50% O_2 50%	28		369	Rhombohedral	3.5
0.40	FZ	Ar 50% O_2 50%	36		371	Rhombohedral	3.4
0.60	FZ	O_2	54		357	Rhombohedral	3.3

were carried out using a pulse magnet. MR was measured with a superconducting magnet in the temperature range of 4.2–400 K. The MR was nearly isotropic, and all the results we presented are for the longitudinal configuration; $I \parallel H$.

III. INSULATOR-METAL PHENOMENA

We show in Fig. 2 temperature dependence of resistivity (ρ) of $La_{1-x}Sr_xMnO_3$ ($0 \leq x \leq 0.4$). Arrows indicate the Curie temperature (T_C) determined by ac susceptibility measurement, which nearly agrees with those of the corresponding ceramics samples.[14] No ferromagnetic phase transition is observed for $x \leq 0.05$. A conspicuous change in ρ is observed at around T_C (downward arrows).

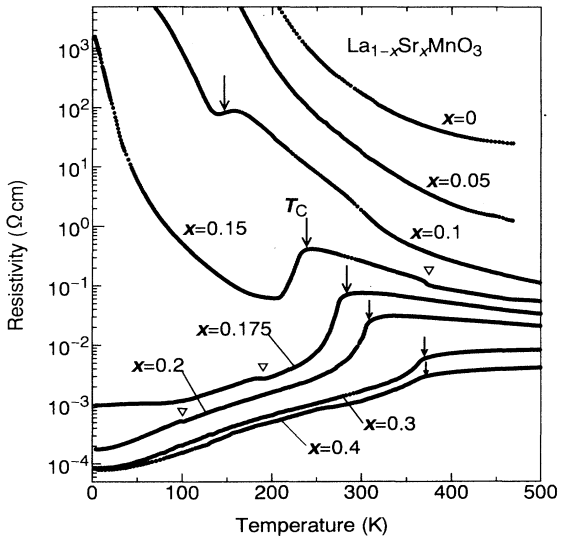

FIG. 2. Temperature dependence of resistivity for $La_{1-x}Sr_xMnO_3$ crystals. Arrows indicate the critical temperature for the ferromagnetic phase transition. Anomalies indicated by open triangles are due to the structural transition (see text).

Above x=0.175, metallic conduction is observed in the low-temperature ferromagnetic phase ($T \leq T_C$). By contrast, ρ at x=0.1 and 0.15 once decreases immediately below T_C, but then, increases due to some localization effects (*vide infra*). In the high-temperature paramagnetic phase ($T \geq T_c$), the $\rho - T$ curve is still characteristic of nonmetal (semiconductor), i.e., $d\rho/dT < 0$, for $x \leq 0.2$. The curve becomes metallic with further increasing x(> 0.3). Anomalies indicated by open triangles for x = 0.15, 0.175, and 0.2 crystals are due to the structural transition from the rhombohedral ($R\bar{3}c$; Z=2) to orthorhombic ($Pbnm$; Z=4) form.[19] These well-defined critical temperatures for the magnetic (T_C) and structural (T_s) transitions ensure the homogeneity of the composition within the sample.

We show in Fig. 3 the correlation between the temperature-dependent changes of ρ and M for various samples with x=0.15, 0.175, 0.2, and 0.3. Because of the

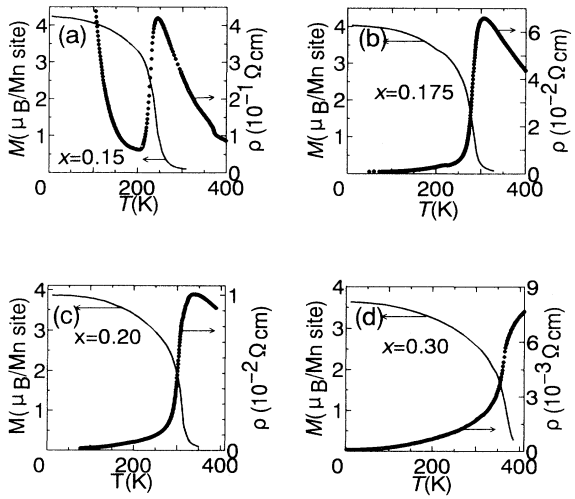

FIG. 3. Correlation between the temperature dependence of resistivity and magnetic moment for $La_{1-x}Sr_xMnO_3$ crystals; (a) x=0.15, (b) x=0.175, (c) x=0.20, and (d) x=0.30. All the data shown were taken with a magnetic field of 0.5 T.

nonremanent behavior of the magnetization in the ferromagnetic phase, the M-T and ρ-T curves were measured with a biased field of 0.5 T. As is clearly seen in Fig. 3, ρ shows a steep decrease in accord with the onset of the ferromagnetic magnetization. Thus, observed temperature dependence of ρ can be interpreted in terms of the carrier scattering by thermal spin fluctuation as well as the decrease of the hole-carrier effective mass.[9–12,18] The electron (hole) transfer (t_{ij}) between the neighboring sites depends on the relative angle ($\Delta\theta_{ij}$) of the local spins in such a manner as $t_{ij}=t_0\cos(\Delta\theta_{ij}/2)$.[12] The ferromagnetic spin arrangement reduces the randomness of the transfer. Semiconducting behavior above T_C for $x \leq 0.175$ [see Figs. 3(a) and 3(b)] may be due to the thermal spin fluctuation and resultant spatial randomness of the transfer interaction (off-diagonal disorder effect).

Contrary to the case near T_C, resistivity in the low-temperature regime (Fig. 4) seems to be governed by the electron-electron scattering process. The spin wave scattering in the ferromagnetic phase[9] is predicted to contribute to the low-temperature resistivity in the form of $T^{9/2}$. As seen in Fig. 4, however, the temperature dependence of the resistivity of the $x = 0.2$–0.4 samples is described such as $\rho(T)=\rho(0) + AT^2$ ($T \leq 200$ K). (A small structure indicated by open triangle is due to the aforementioned structural transition.) The observed T^2 dependence as well as the reduction of the coefficient A with x (see the inset) suggests an important role of the electron-electron scattering process, reflecting the strong electron correlation inherent in the present manganates system.

We summarize in Fig. 5 the electronic phase diagram of $La_{1-x}Sr_xMnO_3$. The low-temperature phase is known to be the spin-canted antiferromagnetic phase for $0 \leq x \leq 0.1$ and ferromagnetic phase $x > 0.1$.[15] The ferromagnetic transition temperature T_C (filled triangles) increases with x and reaches the maximum ($\approx$ 370 K) around x=0.4. The critical temperatures for the antiferromagnetic (T_N) and ferromagnetic (T_C) phase transition are listed in Table I. We may classify the electronic phase into the following five categories according to the spin configuration and the electrical conduction: Below the magnetic transition temperature, the three phases are present; a spin-canted antiferromagnetic insulator (CNI) in the low-doped region ($x < 0.1$), a ferromagnetic insulator (FI) in the region of $0.1 \lesssim x \lesssim 0.15$, and a ferromagnetic metal (FM) in the high-doped region of $x > 0.15$. Above the magnetic transition temperatures (T_N and T_C), on the other hand, the nonmetal (PI)-to-metal (PM) transition appears to occur around $x = 0.3$.

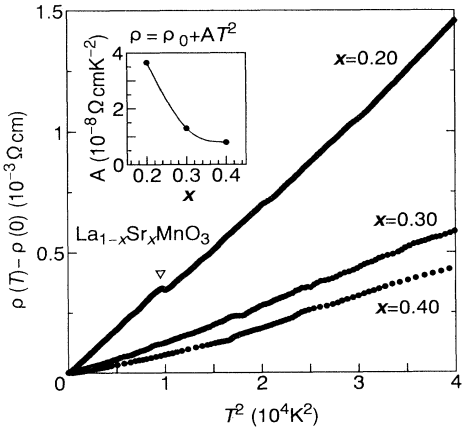

FIG. 4. Temperature dependence of resistivity in the low-temperature region ($\leq$200 K) for $La_{1-x}Sr_xMnO_3$ crystals. The T^2 dependence of resistivity $[\rho(T)=\rho(0)+AT^2]$ was observed. Inset shows the coefficient A against the nominal hole concentration x. An open triangle represents the structural transition (see text).

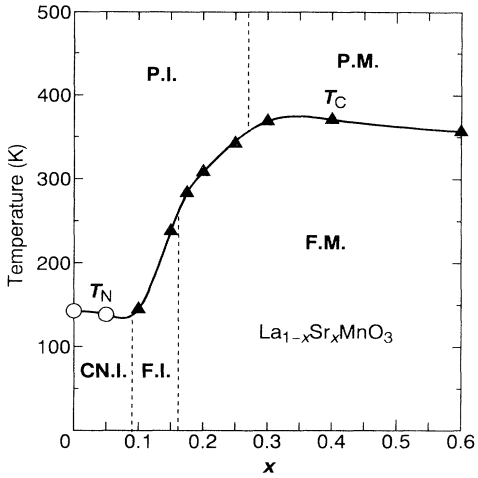

FIG. 5. Electronic phase diagram of $La_{1-x}Sr_xMnO_3$. Open circles and filled triangles are the Néel (T_N) and Curie (T_C) temperatures, respectively. The abbreviations mean paramagnetic insulator (PI), paramagnetic metal (PM), spin-canted insulator (CNI), ferromagnetic insulator (FI), and ferromagnetic metal (FM).

Among these five phases, the FI phase is to be further mentioned, since a simple theory considering the double exchange interaction predicts only the metallic ferromagnetic phase at low temperature. The less itinerant conduction electron is amenable to localization effect due to the random impurity (i.e., substituted Sr ions) potential or the electron-lattice interaction. Application of hydrostatic pressure ($\sim$ 1 GPa) and resultant increase of the itineracy makes the system metallic down to zero temperature, nearby the filling-induced insulator-metal phase boundary ($x_c \sim 0.17$).[20] Even the localized carriers, which cannot contribute to the macroscopic charge transport, may mediate the ferromagnetic interaction between the neighboring local spins to cause the ferromagnetic phase in a bond-percolative manner.

IV. MAGNETORESISTANCE

On the basis of the observed correlation between the resistivity change and the onset of the net magnetization (Fig. 3), an intuitive view on the MR effect is obtained to be as follows: The applied magnetic field tends to align the local spin and reduces the spin scattering of the con-

duction electron. In Fig. 6, we show the magnetic field effect on the resistivity (the longitudinal MR; $I \parallel H$) for (a) $x = 0.15$, (b) $x = 0.175$, and (c) $x = 0.20$. The MR was found to be nearly isotropic; the transverse MR is only a few percent smaller in the absolute magnitude than the longitudinal MR possibly due to diamagnetic correction effect. Large negative MR is observed around T_C for all the samples. The negative MR value defined as $-[\rho(H) - \rho(0)]/\rho(0)$ is also plotted in Fig. 6 by open circles with a field of $\mu_0 H = 15$ T. The MR value becomes as large as 0.95 around 240 K in the $x = 0.15$ sample [Fig. 6(a)]. Together with the change in sign of the temperature gradient of ρ, the observed MR phenomena immediately above T_C may be interpreted as a field-induced nonmetal-metal transition. Incidentally, anomalies in the MR curves (open triangles) are due to the rhombohedral-to-orthorhombic structural transition. The observation indicates the field-induced shift of T_s toward the low-temperature side. This phenomenon as well as its mechanism are described in a separate publication.[19] Let us focus here on the overall features of the MR correlated with the field-induced magnetization (M).

We show in Fig. 7 the correlation between the field-induced changes in ρ and M for (a) x=0.15 and (b) the x=0.175. As clearly seen, the magnitude of the MR cor-

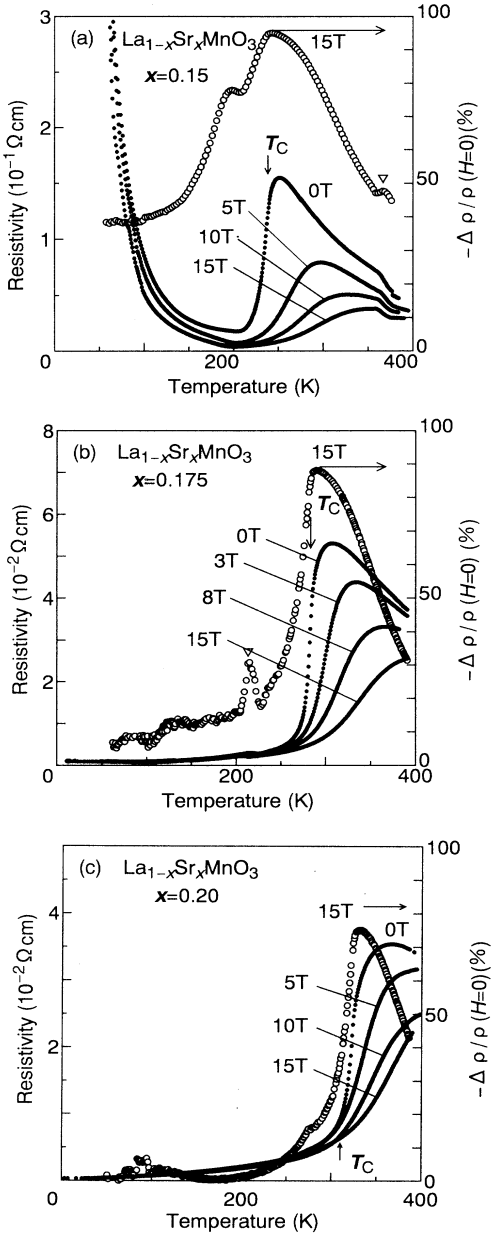

FIG. 6. Temperature dependence of resistivity for $La_{1-x}Sr_xMnO_3$ crystals under various magnetic fields; (a) x=0.15, (b) x=0.175, and (c) x=0.20. Open circles represent the magnitude of negative magnetoresistance $-[\rho(H) - \rho(0)]/\rho(0)$ with a magnetic field of 15 T. Open triangles represent the structural transitions (see text).

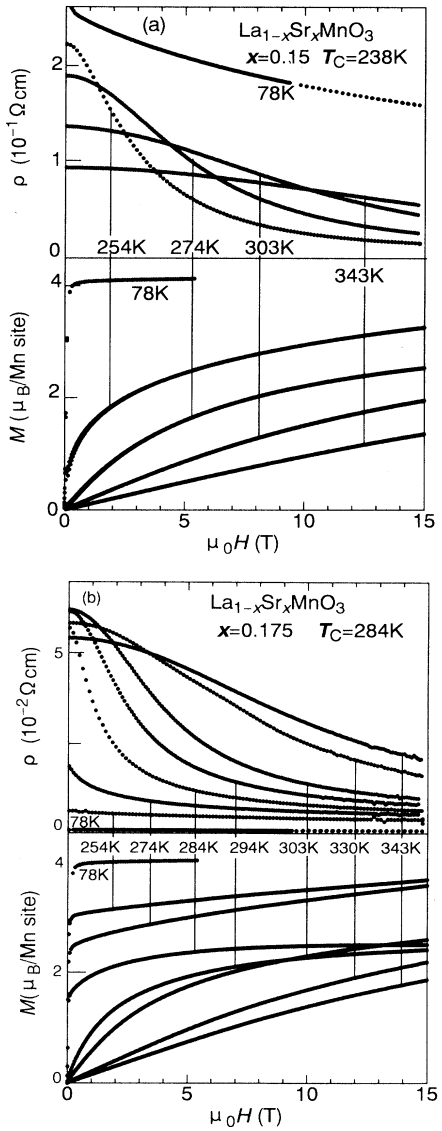

FIG. 7. Reduction of the resistivity (upper panels) and magnetization (lower panels) with an external magnetic field for $La_{1-x}Sr_xMnO_3$ crystals; (a) x=0.15 and (b) x=0.175.

relates with the change in M; the MR is large around T_C but is very small far below T_C, for example, at 78 K at x=0.175 [see Fig. 7(b)]. [The rapid rise of the magnetization curve in the low-temperature phase ($T \ll T_C$) is due to the domain motion in the present soft ferromagnet, which least affects the ρ value.] For the semiconducting (but ferromagnetic) x=0.15 sample [Fig. 7(a)], however, the MR effect seems to persist at 78 K where the magnitude of M is readily saturated with a nearly classical value ($\approx 4\mu_B$) above $\sim$ 0.2 T. This is perhaps related to the Anderson localization of the fully spin polarized e_g carriers. Nevertheless, the MR shows minimal anisotropy for the longitudinal and transverse field configurations. This phenomenon is left to be clarified.

With use of the M-H and ρ-H curves at respective temperature, we have deduced the change of the resistivity as a function of M. The net magnetization represents the averaged ordered moment of sum of the t_{2g} spins and the forcedly aligned e_g spin on the identical Mn site. The results for the x=0.175 sample are shown in Fig. 8, in which the magnetization on the abscissa is normalized by the classical value (M_S=$4\mu_B$) in the case of the n=1 filling of the e_g band. Looking at the ρ-M curve, one may notice that the experimental points taken at different temperatures above T_C show an approximately identical curve in spite of seemingly different MR behaviors [see Fig. 7(b)]. In Fig. 8 is also shown the ρ-M curve, which was obtained by the temperature dependence of the ρ and M data taken at a field of 0.5 T [see Fig. 3(b)]. The curve shows a similar trace to the universal curve obtained from the field dependence. The good coincidence suggests that the ρ-T curve is also governed by a similar scattering process to the case of the MR. The experimental points taken below T_C draw horizontal lines (dashed lines) in the low-M region, but merge to the universal curve in the high-M region ($M \sim M_s$). In other words, the initial magnetization governed by the domain wall displacement (typically below 0.2 T) does not represent the magnitude of the field-induced moment on the respective Mn site, and hence does not influence the carrier scattering process. A small but systematic discrepancy between the temperature-variational and field-variational curves is observed in the high-M region. This is likely contributed from the temperature-dependent scattering process, such as electron-electron (see Fig. 4) and electron-phonon scattering. Furthermore, the effect of the quantum fluctuation of the local spin may play some role in the carrier scattering because of extremely strong mutual coupling.

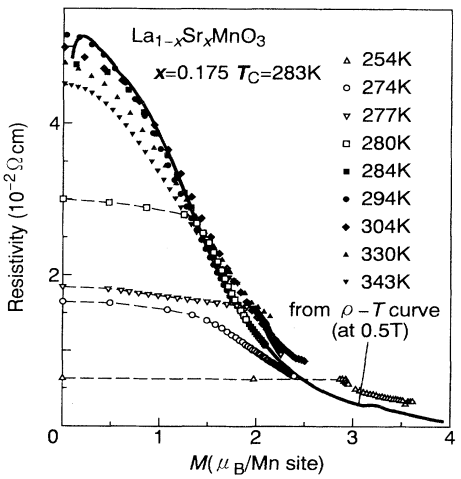

FIG. 8. Change of the resistivity as a function of magnetization for $La_{1-x}Sr_xMnO_3$ crystal (x=0.175). The points are obtained from the ρ-H and M-H curves at respective temperatures. The solid line is obtained using the ρ-T and M-T curves with a biased field of 0.5 T.

Finally, let us show the result for the filling-dependence of the MR effects. In Fig. 9 we plot the negative MR value $-[\rho(H)-\rho(0)]/\rho(0)$ measured immediately above T_C (at $1.01T_C$ and $1.05T_C$) against $(M/M_S)^2$ for x=0.175, 0.3, and 0.4. As is seen in Fig. 9, M dependence of the MR value is well expressed by a scaling function:

$$-[\rho(H)-\rho(0)]/\rho(0) = C(M/M_s)^2, \quad (1)$$

at least in the relatively low-M region, say $M \leq 0.3M_s$. One may notice that the coefficient C remarkably depends on the x value. The scaling constant C is rather high, about 4, near the metal-insulator phase boundary (indicated by an arrow in the inset), but steeply decreases with x and become $\sim$1 at x=0.4 (see the inset).

Concerning the MR magnitude as scaled by Eq. (1), there have been several theoretical investigations on the basis of the s-d model Hamiltonian or Kondo-lattice Hamiltonian with ferromagnetic coupling ($J \geq 0$).[9,18] For example, the calculation using the phenomenological

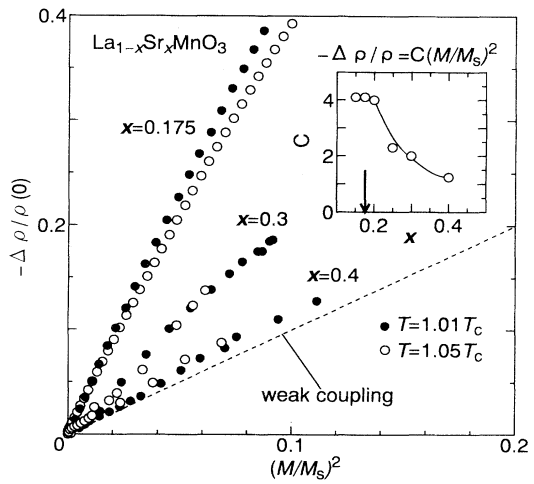

FIG. 9. Magnitude of magnetoresistance $-\Delta\rho/\rho(0)$ as a function of $(M/M_s)^2$ for $La_{1-x}Sr_xMnO_3$ crystals. Filled and open circles are at T=$1.01T_C$ and T=$1.05T_C$, respectively. A dashed line represents the theoretical curve in the weak-coupling limit of the Kondo-lattice model (see text). Inset shows the x dependence of the scaling constant C in the relation that $-\Delta\rho/\rho(0) = C(M/M_s)^2$ at $T = 1.01T_C$. A downward arrow indicates the compositional insulator-metal boundary ($x_c \sim 0.17$).

Drude-like assumptions[9] predicts $C=1$ in the case of the present manganates ($S=2$). Recently, Furukawa[18] has calculated the constant C as a function of the band filling $n(=1-x)$ and the coupling strength (Hund energy) J using Kubo formula in the limit of $S=\infty$ (i.e., classical spin) and infinite dimension ($D=\infty$). He showed that the calculated value of C can exceed unity, e.g., about four in the case of the strong coupling where J is much larger than the one-electron bandwidth W, but becomes $C \sim 1$ in the weak coupling limit. The presently observed results clearly indicate that the decrease (increase) of the band filling n (nominal hole concentration x) drives the system effectively towards the weak coupling regime.

V. SUMMARY

With use of melt-grown crystals of $La_{1-x}Sr_xMnO_3$, we have investigated the transport and magnetic properties relating to the insulator-metal transition driven by carrier-doping and clarified the correlation between them. Large negative MR phenomena were observed near the critical temperature T_C for the ferromagnetic phase transition. Magnetic field-dependent as well as temperature-dependent resistivity is well scaled with M. In the relatively low-M region ($M \leq 0.3M_s$, M_s being the saturation moment of ca. $4\mu_B$), the negative MR value is well described as $-\Delta\rho/\rho(0)=C(M/M_s)^2$ over the whole range of x. The x dependence of the coefficient C indicates that the hole-doping procedure drives the system towards the weak coupling regime. The mean-field-type theory for the ferromagnetic Kondo-lattice model explains why the coefficient C (or the MR magnitude in the low-M region) can be so large ($C \sim 4$), yet effect of the quantum fluctuation of the local spins should be taken into account for the quantitative understanding of the MR phenomena in the high-M region as well as of the low-temperature transport properties.

ACKNOWLEDGMENTS

The authors are grateful to N. Furukawa for enlightening discussions. We also thank J. Akimitsu and K. Tomimoto for their help in the EPMA, H. Yoshizawa for the neutron diffraction characterization of the crystals, and T. Hamamoto for his help in the high-magnetic field experiment. This work was supported by New Energy and Industrial Technology Development Organization (NEDO) and by a Grant-In-Aid for Scientific Research from the Ministry of Education, Science, and Culture, Japan.

* Author to whom correspondence should be addressed.

[1] For a review, see, J.B. Goodenough and J.M. Longon, *Magnetic and Other Properties of Oxides and Related Compounds*, edited by K.-H. Hellwege and O. Madelung, Landolt-Börnstein, New Series, Group III, Vol. 4, Pt. a (Springer-Verlag, Berlin, 1970).
[2] R.M. Kusters, D.A. Singleton, D.A. Keen, R. McGreevy, and W. Hayes, Physica B **155**, 362 (1989).
[3] K. Chabara, T. Ohno, M. Kasai, and Y. Kozono, Appl. Phys. Lett. **63**, 1990 (1993).
[4] R. von Helmolt, J. Wocker, B. Holzapfel, M. Schultz, and K. Samwer, Phys. Rev. Lett. **71**, 2331 (1993).
[5] S. Jin, T.H. Tiefel, M. McCormack, R.A. Fastnacht, R. Ramesh, and L.H. Chen, Science **264**, 413 (1994).
[6] H.L. Ju, C. Kwon, R.L. Greene, and T. Venkatesan, Appl. Phys. Lett. **65**, 2108 (1994).
[7] M. McCormack, S. Jin, T.H. Tiefel, R.M. Fleming, and Julia M. Phillips, Appl. Phys. Lett. **64**, 3045 (1994).
[8] Y. Tokura, A. Urushibara, Y. Moritomo, T. Arima, A. Asamitsu, G. Kido, and N. Furukawa, J. Phys. Soc. Jpn. **63**, 3931 (1994).
[9] K. Kubo and N. Ohata, J. Phys. Soc. Jpn. **33**, 21 (1972).
[10] C. Zener, Phys. Rev. **82**, 403 (1951).
[11] P.-G. de Gennes, Phys. Rev. **118**, 141 (1960).
[12] P.W. Anderson and H. Hasegawa, Phys. Rev. **100**, 675 (1955).
[13] T. Arima, Y. Tokura, and J.B. Torrance, Phys. Rev. B **48**, 17 006 (1993).
[14] G.H. Jonker and J.H. Van Santen, Physica **16**, 337 (1959); **16**, 337 (1959).
[15] E.O. Wollan and W.C. Koehler, Phys. Rev. **100**, 545 (1955).
[16] For a review at an early stage of experimental works on perovskite manganese oxides, see, G.H. Jonker, Physica **22**, 707 (1956).
[17] C.W. Searle and S.T. Wang, Can. J. Phys. **47**, 2023 (1969).
[18] N. Furukawa, J. Phys. Soc. Jpn. **63**, 3214 (1994).
[19] A. Asamitsu, Y. Moritomo, Y. Tomioka, T. Arima, and Y. Tokura, Nature **373**, 407 (1995).
[20] Y. Moritomo and Y. Tokura (unpublished).